Constitutive parameters, mechanical properties and failure mechanism in DC-cast AA7050 billets

M. Lalpoor[1], D.G. Eskin[1] and L. Katgerman[2]
[1] Materials Innovation Institute. Mekelweg 2, 2628 CD Delft, The Netherlands
[2] Delft University of Technology, Department of Materials Science and Engineering, Mekelweg 2, Delft, 2628 CD, The Netherlands

Abstract

Brittleness of 7xxx series aluminum alloys in the as-cast condition along with the accumulation of thermal stresses during solidification results in catastrophic failure of direct-chill (DC) cast billets. Since these alloys are usually used after deformation and heat treatment, very little research has been performed on their mechanical behavior in the as-cast condition. In this study mechanical properties of a cylindrical DC-cast AA7050 billet (255mm diameter) were examined along its axial and radial directions, at different temperatures and strain rates. Tensile tests over the post-solidification temperature range (20–400 ºC) revealed that the sudden fall in the material ductility (from 23% to 2.5%) below 300 ºC was typical of all examined billet sections and was the result of grain boundary embrittlement. Constitutive parameters derived from the true stress–strain curves, supported the former findings that below 200 ºC material's behavior became strain-rate independent.

1. Introduction

Direct-chill (DC) semicontinuous casting of axis-symmetric billets is one of the most important stages in the production of aluminum alloys. A major problem however is the formation of residual stresses which can cause cold cracking [1]. Cold cracks which occur in a fully solid material propagate as a result of further increase of thermal stresses in the solid state accompanied by weaker mechanical properties of the alloy in certain temperature ranges [2,3].

Non-equilibrium cooling rates and solidification conditions in different locations of DC-cast billets can affect the mechanical properties of the material in several ways. Microsegregation of solute elements (Zn, Mg and Cu) during non-equilibrium solidification results in the formation of non-equilibrium eutectic phases [4, 5]. Formation of such intermetallic phases as $(AlCuZn)_2Mg$, Al_2CuMg and $Al_2Mg_3Zn_3$, mainly in the final stages of solidification, in inter-dendritic spaces and on grain boundaries results in the brittleness of the material. Other constituent phases (Al_7Cu_2Fe and Mg_2Si [3]) formed by impurity elements (Fe and Si) also increase the materials susceptibility to cracking, but their volume fraction and effect are less than those of larger intermetallics present in the microstructure. Temperature gradients during DC casting and different thickness of the transition (liquid–solid) region across the ingot cross-section also lead to the variation in microstructural features (grain size, dendrite arm spacing, fraction and size of constitutive particles), composition (macrosegregation) and defects (porosity and hot cracks) [6]. These inhomogeneities produce different mechanical properties [7] in different ingot sections and may cause different susceptibility of the material to cracking.

All these microstructural defects act as stress raisers in the presence of residual thermal stresses, and their random size, shape and distribution make it difficult to predict cracking in DC-cast billets. Brittleness of the material in the as-cast condition on the other hand has prevented researchers from performing the mechanical tests on such alloys in the pure as-cast condition. This is, however quite necessary for the numerical simulation of thermal stresses and strains in the solidifying billets.

In this paper the mechanical properties of a DC-cast AA7050 billet are measured along its radial and axial directions in the as-cast condition over a wide range of subsolidus temperatures. Constitutive parameters of the alloy are also extracted to be used for the thermo-mechanical simulation of stresses. The structure and fractures are examined in an attempt to interpret the results of mechanical testing.

2. Experimental procedure

The material used in this research work was AA7050 billet produced by DC casting with a conventional mold from the melt that was degassed in the furnace and supplied by Corus-Netherlands (IJmuiden). Chemical composition of the alloy in terms of wt% is as follows: Zn: 6.3, Mg: 2.42, Cu: 2.49, Zr: 0.098, Ti: 0.03, Fe: 0.07, Si: 0.04, Mn: 0.04 and Cr: <0.01.

Tensile mechanical properties of the as-cast 7050 samples were measured using a Gleeble-1500 thermomechanical simulator. Samples were cut from a cylindrical billet with a diameter of 255 mm along its radial and axial (vertical) direction. Axial samples were cut 10 mm off the surface, at the mid-radius and center of the billet to investigate the mechanical properties of the material at different distances from the center. Radial samples were extracted from the middle of the radius to determine the constitutive parameters. Tensile specimens were heated through the Joule effect at a rate of 10 ºC/s, kept for 10 seconds and then uniaxially deformed at three strain rates of 10^{-2}, 10^{-3} and 10^{-4} s^{-1} (only 10^{-2} s^{-1} for the axial samples). The range of strain rates was chosen to resemble those typical of DC casting [8]. Mechanical properties were measured from room temperature to 400 ºC at 100 ºC steps for radial samples and at 200 ºC steps for axial ones. Four samples were tested for each specific temperature and strain rate combination, and the average values are reported. Fracture surfaces were preserved for fractographical investigations.

Grain size and dendrite arm spacing were measured based on ASTM-E112. For this purpose samples were polished using diamond suspensions (up to 1 μm) and then anodized in a diluted solution of HBF_4 acid (3%) in distilled water, grains were then revealed using polarized light in an optical microscope Neophot 30. A scanning electron microscope Jeol JSM-6500F (SEM) and the optical microscope (OM) were used for structure and fracture observations. Qualitative and quantitative chemical compositions of the phases present on the fracture surfaces were estimated using backscattered electron detector (BSE) and energy dispersive spectra (EDS) in the SEM. Electron backscattered images of the samples were also analyzed using the image analysis software Image J to measure the volume fraction of the non-equilibrium phases.

3. Results

3.1. Samples along the radial direction

The true stress-strain curves of the radial samples at five temperatures under a strain rate of 10^{-4} s^{-1} are shown in Fig. 1. As temperature falls below 400 ºC, the material starts to behave more brittle and shows less ductility. The alloy loses its ductility below 200 ºC and fails in a brittle manner, which is accompanied by a higher fracture strength. The yield (fracture) strength reaches 279 MPa at room temperature and falls to 30 MPa as the temperature increases to 400 ºC. Figures 2 and 3 show the effect of temperature on yield strength and ductility (% elongation). Similar behavior is observed: with the material becoming quite brittle below 200 ºC (same trend was observed for reduction in area values). The yield strength increases as the temperature decreases in a linear manner.
The effect of strain rate on the flow stress of the 7050 alloy at the true strain 0.002 is shown in Fig. 4. At high temperatures (300 and 400 ºC) the flow stress increases as the deformation rate increases, but at lower temperatures (beginning at 200 ºC) the material behavior becomes strain-rate independent.

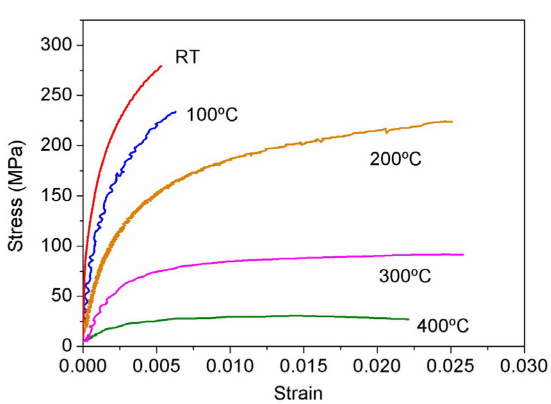

Fig. 1 Examples of true stress–strain curves for 7050 samples (cut along the radial direction) tested at different temperatures at a strain rate of 10^{-4} s^{-1}. Similar trends were observed for the other strain rates.

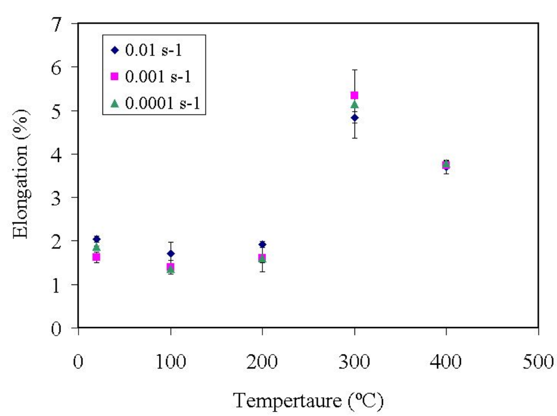

Fig. 2 Average elongation of 7050 samples cut along the radial direction of the billet tested at different temperatures and strain rates.

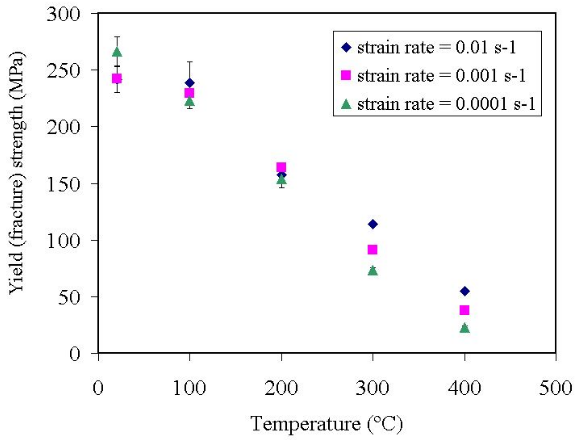

Fig. 3 Average yield (fracture) strength of 7050 samples cut along the radial direction tested at different temperatures and strain rates.

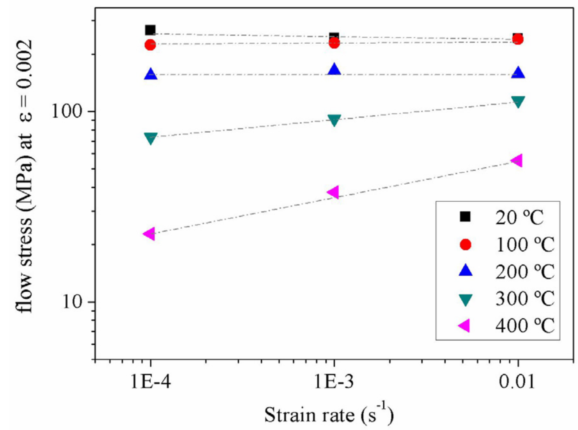

Fig. 4 Effect of strain rate on the yield (fracture) strength for 7050 samples cut along the radial direction tested at different temperatures.

3.1. Samples along vertical billet axis

Figure 5 shows the yield strength of the alloy versus distance from the center of the billet. As can be seen at 200 and 400 ºC yield strength value is almost independent of the location in the billet. At room temperature on the other hand, the highest yield strength appears in the middle of the billet radius. The scattering in the results is highest for the samples near to the surface of the billet. Figure 6 shows the elongation profile along the radius of the billet. One notices that below 200 ºC the material becomes brittle with elongation values around 2%. At 400 ºC the curvature of the changes reverses, with the highest and lowest ductility in the center and surface of the billet respectively. The scattering in the results are also higher at these two locations.

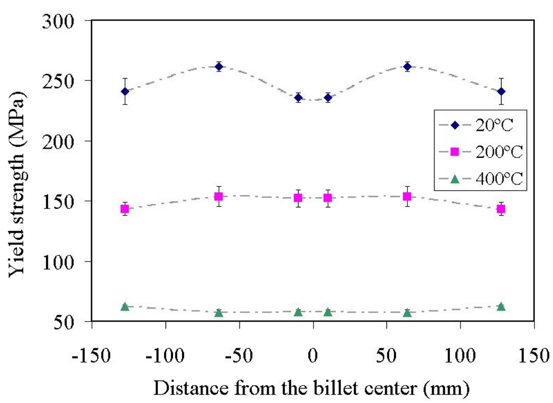

Fig. 5 Yield (fracture) strength for the samples cut along the axial direction of the billet at three different locations. Results are shown for three different temperatures and a strain rate of 10^{-2} s^{-1}.

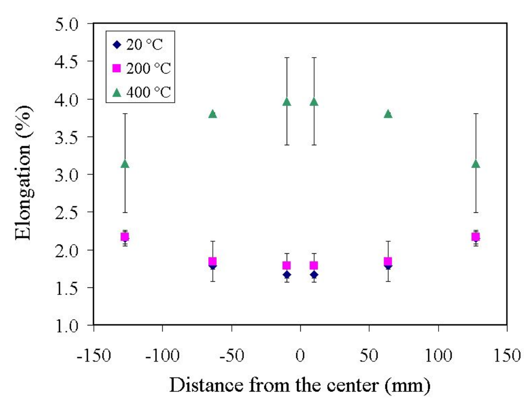

Fig. 6 Elongation (%) for the samples cut along the axial direction of the billet at three different locations. Results are shown for three different temperatures and strain rate of 10^{-2} s^{-1}.

3.2. Constitutive parameters

In order to simulate the DC-casting process from solidus temperature to room temperature suitable equations describing the material's mechanical behavior are required. One approach is the extended Ludwik equation:

$$\sigma = K(T)(\varepsilon_p + \varepsilon_p^0)^{n(T)}(\dot{\varepsilon}_p)^{m(T)} \qquad (1)$$

K(T) is the consistency of the alloy, *n*(T) is the strain hardening coefficient, *m*(T) is the strain rate sensitivity, and ε_p^0 is a constant equal to 0.001[9]. The true stress-strain curves of the material were fitted to Eq. 1 to determine *K*(*T*), *n*(*T*) and *m*(*T*), whose values are shown in Table 1. As can be seen the values of *K* and *n* decrease as the temperature increases, whereas the *m* values increase with temperature. *m* values appear to be negative below 200 ºC.

Table 1. Constitutive parameters of the 7050 alloy determined from the extended Ludwik equation.

Temperature (ºC)	*K* (MPa)	*n*	*m*
20	774 ± 32	0.42 ± 0.02	–0.2 ± 0.02
100	626 ± 13	0.38 ± 0.01	–0.16 ± 0.03
200	392 ± 11	0.21 ± 0.006	–0.03 ± 0.005
300	199 ± 4.5	0.11 ± 0.007	0.03 ± 0.007
400	174 ± 5	0.09 ± 0.01	0.15 ± 0.009

3.2. Structure examination

Quantitative metallographic results are shown in Table. 2. As it can be seen the grain size increases from the surface to the center of the billet. Same trend is observed for dendrite arm spacing (DAS), but it does not vary between the mid-radius and center of the billet. The amount of non-equilibrium constituents was measured based on image analysis of the BSE images (using Image J software) and the results are also shown in Table 2. Volume fraction of non-equilibrium eutectics remains more or less the same in the center of the billet and at the mid-radius but there is a slight increase as we move from the mid-radius to its surface.

Table 2. Microstructural features of the 7050 alloy.

Location in the billet	Grain size (μm)	DAS (μm)	Fraction of eutectics (%)
Centre	229 ± 6	34 ± 1.4	4.5 ± 0.17
Middle radius	179 ± 4	28 ± 0.9	4.6 ± 0.11
Surface	130 ± 2	28 ± 1.0	4.9 ± 0.08

4. Discussion

Detailed examination of fracture surfaces in SEM revealed that the material fails in interdendritic manner (Fig. 7a) and the fracture mode of samples was similar regardless of their position in the billet. Non-equilibrium phases and intermetalics on the fracture surfaces lead to failure in two ways: either by cleavage (Fig. 7b) in presence of resolved normal stresses on them, or decohesion from the matrix (Fig.7c) as a result of their weak bonding to it. Presence of intermetallic phases in interdendritic spaces results in grain boundary embrittlement and finally decohesive rupture of the material. Fe-rich regions found on the top of the outward projecting dendrite arms or at the bottom of the valleys on the fracture surface show how Al_7Cu_2Fe particles can act as stress raisers or crack initiators in the microstructure (Fig.7b). Another feature of fracture surfaces is the presence of fractured interdendritic bridges which fail when the cracks fast propagating through the intermetallics reach them (Fig 7d) which was also observed by Katgerman *et. al* on hot crack surfaces of a 7050 alloy [10].

Comparison of the results gained for yield strength and ductility with those gained for stress relieved [11] and homogenized [7] billets shows that the material is more brittle in the pure as-cast condition without any stress-relieving treatment. Material's low ductility below 200 ºC (≤ 2%) appears to be the main reason for the high susceptibility to cold cracking, the fact which is in agreement with the conclusions of Livanov *et. al* [12] that cold cracking does not occur when the tensile elongation of the material exceeds 1.5%. Another consequence of brittleness which makes the material more prone to cracking is that below 200 ºC materials behavior becomes strain rate independent (Fig.4). Local increase of the stresses in the billet accompanied by a rise in their value (by micro cracks or defects) can result in catastrophic failure of the billet.

Relatively uniform grain size and DAS in the cross-section of the billet has resulted in similarities in the mechanical properties (taking the scattering of the results into account) regardless of the location on the radial axis. Hence, presence of continuous non-equilibrium phases on the boundaries and inter-dendritic spaces appeared to be the main failure reason in this study. Existence or instantaneous formation of any microcrack in one of these regions can result in catastrophic failure in the presence of residual stresses. This might apparently exclude the influence of microstructural features as grain size or DAS on the failure of the billet in this study, Which is not the case in larger billets where accumulation of thermal stresses during solidification accompanied by critical low mechanical properties (e.g. ductility) at some critical positions of the billet (with critical grain size or DAS) might lead to failure.

Comparing the constitutive parameters determined in this research work with stress relieved 7050 DC-cast billets [11] reveals some differences. K and n values are higher at temperatures below 200 ºC and decrease in a linear manner as the temperature falls, but in stress-relieved samples these dependences pass first through a plateau up to 200 ºC and then fall.

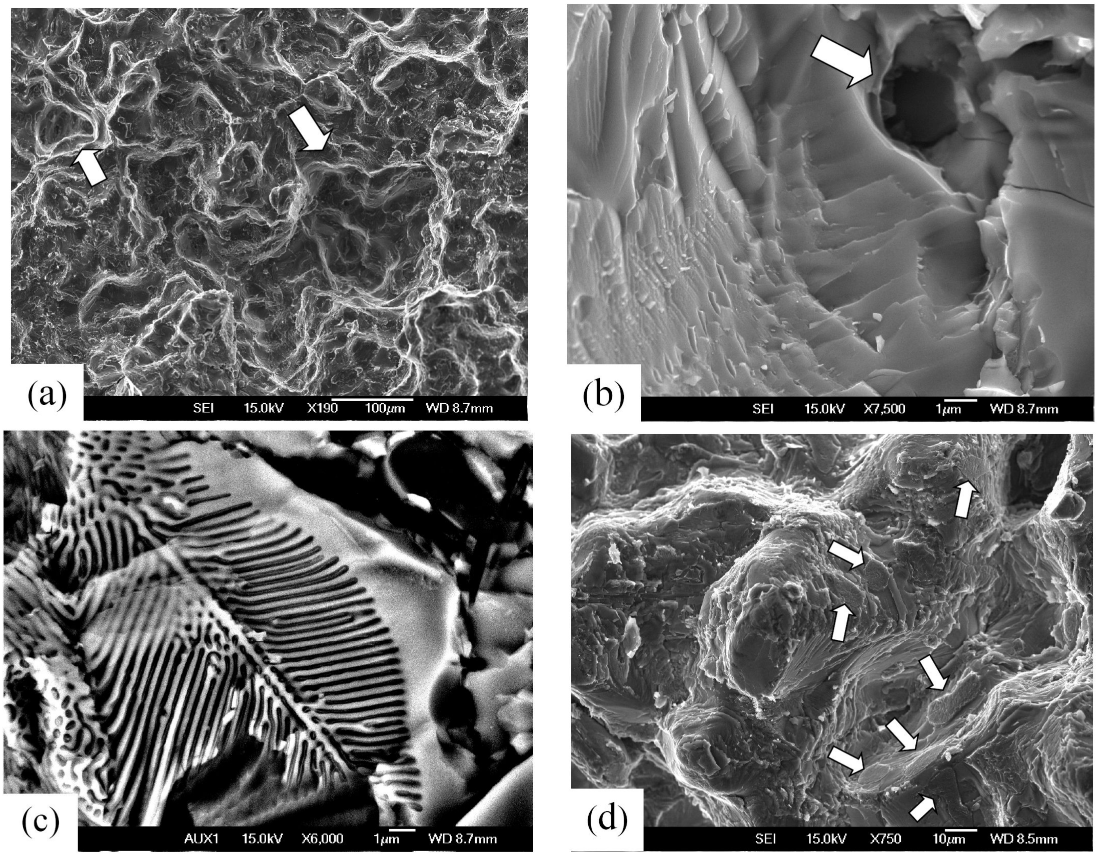

Fig. 7 Fracture surfaces in a 7050 alloy: (a) sample from the middle radius of the billet failed at room temperature at the strain rate of 10^{-2} during tensile test. Arrows show the dendrites failed through decohesion; (b) the same sample as (a) but in higher magnification showing the cleavage in side walls of a dendrite arm. Arrow shows the probable crack initiation site, which appeared to be a Fe rich particle; (c) electron backscattered image of the sample from the surface of the billet failed at 200 ºC at the strain rate of 10^{-2} during tensile test; and (d) the same sample as (a) showing the outward standing dendrite arms with broken side bridges on them. Arrows show the broken (cleaved?) interdendritic bridges, SEM.

5. Conclusions

Room and high temperature tensile tests were performed on DC-cast AA7050 alloy to reveal the materials behavior in the as-cast condition over the post solidification temperature range. Within this range, the lower the temperature, the more brittle is the material, the less strain-rate dependent are the mechanical properties, and the higher is the probability of the failure before reaching the yield point. Investigation of the fracture surfaces revealed that the grain boundary embitterment leads to the brittleness of the material and eventually results in decohesive rupture. Detrimental effect of non-equilibrium eutectic phases on the mechanical properties arises from their continuous presence along grain boundaries and inter-dendritic spaces. Constitutive parameters of the material were also derived in this temperature range using the extended Ludwik equation. Using such parameters for numerical thermal stress/strain analysis would result in a more realistic explanation of material's thermomechanical behavior during DC-casting.

Acknowledgments

This research was carried out under the project number 05237 in the framework of the Research Program of the Materials Innovation Institute (www.m2i.nl), former Netherlands Institute for Metals Research. Fruitful discussions with Dr. W. Boender and Dr. A. Ten Cate (Corus RD&T) are appreciated. Authors would like also to thank Corus Netherlands (IJmuiden) for providing material for the research.

References

[1] H.G. Fjaer and A. Mo, ALSPEN-A mathematical model for thermal stresses in direct chill casting of aluminum billets, Metallurgical Transactions B 21B (1990) 1049-1061.
[2] R.K. Paramatmuni, Keh-Minn Chang, Bruce S. Kang, X. Liu, Evaluation of cracking resistance of DC casting high strength aluminum ingots, Materials Science and Engineering A 379 (2004) 293–301.
[3] Q. Han, S. Viswanathan, D.L. Spainhower, S.K. Das, Nature and formation of surface cracks in DC cast ingots, Metallurgical and Materials Transactions A 32A (2001) 2908–2910.
[4] F. Xie, X. Yan, L. Ding, F. Zhang, S. Chen, M. G. Chu, Y. A. Chang, A study of microstructure and microsegregation of aluminum 7050 alloy, Materials Science and Engineering A355 (2003) 144-153.
[5] S.T. Lim, Y.Y. lee and II-Sang Eun, Dilute alloy designs of 7xxx aluminum alloys for thick forging applications, Materials Science Forum 475-479 (2005) 369-372.
[6] D.A. Granger, Ingot Casting in the Aluminum Industry. (Retroactive Coverage), in: A.K. Vasudevan, R.D. Doherty (Eds.), Aluminum Alloys–Contemporary Research and Applications, Academic Press, London, 1989, pp. 109-135.
[7] J. Wan, H.M. Lu, K. M. Chang, J. Harris, As-cast mechanical properties of high strength aluminum alloy, in: B. Welch (Ed.), Light Metals 1998, TMS, Warrendale, 1998, pp. 1065-1071.
[8] W.M. van Haaften, Constitutive Behavior and Hot Tearing during Aluminum DC Casting, PhD thesis, Delft University of Technology, Delft Press, Delft, 2002, pp. 11–38.
[9] B. Magnin, L. Katgerman, B. Hannart, Physical and numerical modeling of thermal stress generation during DC casting of aluminum alloys, in: M. Cross and J. Campbell, (Eds.), TMS MCWASP VII, Warrendale, USA 1995, pp.303-310.

[10] L. Katgerman, W.M. van Haaften, and W.H. Kool, Constitutive Behaviour and Hot Tearing during Aluminium DC Casting, Materials Forum 28 (2004) 312-318.
[11] K.-M. Chang, H.-M. Lu, J. Wan, in: Second Intern. Conf. on Quenching and Control of Diffusion, ASM International, Ohio, 1996, pp. 341–345.
[12] V.A. Livanov, R.M. Gabidullin, V.S. Shipilov, Continuous casting of aluminum alloys, Metallurgiya, Moscow, 1977, p.90.